

See discussions, stats, and author profiles for this publication at: <https://www.researchgate.net/publication/51669853>

# Nanostructured Titanium/Diamond-Like Carbon Multilayer Films: Deposition, Characterization, and Applications

ARTICLE in ACS APPLIED MATERIALS & INTERFACES · SEPTEMBER 2011

Impact Factor: 6.72 · DOI: 10.1021/am200939j · Source: PubMed

---

CITATIONS

26

---

READS

55

## 3 AUTHORS, INCLUDING:



Sushil Kumar

National Physical Laboratory - India

100 PUBLICATIONS 972 CITATIONS

[SEE PROFILE](#)



Hitendra Malik

Indian Institute of Technology Delhi

157 PUBLICATIONS 1,185 CITATIONS

[SEE PROFILE](#)

# Nanostructured Titanium/Diamond-Like Carbon Multilayer Films: Deposition, Characterization, and Applications

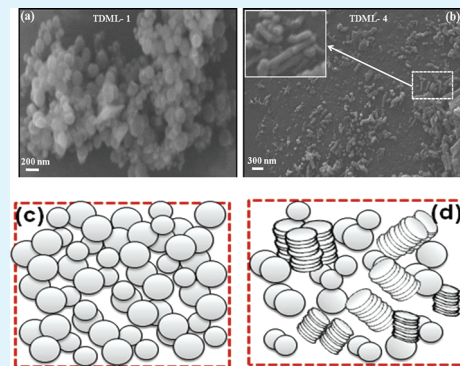
Neeraj Dwivedi,<sup>†,‡</sup> Sushil Kumar,<sup>\*,†</sup> and Hitendra K. Malik<sup>‡</sup>

<sup>†</sup>Physics of Energy Harvesting Division, National Physical Laboratory (CSIR), K.S. Krishnan Road, New Delhi, 110 012, India

<sup>‡</sup>Department of Physics, Indian Institute of Technology Delhi, New Delhi, 110 016, India

**ABSTRACT:** Titanium/diamond-like carbon multilayer (TDML) films were deposited using a hybrid system combining radio frequency (RF)-sputtering and RF-plasma enhanced chemical vapor deposition (PECVD) techniques under a varied number of Ti/diamond-like carbon (DLC) bilayers from 1 to 4, at high base pressure of  $1 \times 10^{-3}$  Torr. The multilayer approach was used to create unique structures such as nanospheres and nanorods in TDML films, which is confirmed by scanning electron microscopy (SEM) analysis and explained by a hypothetical model. Surface composition was evaluated by X-ray photoelectron spectroscopy (XPS), whereas energy dispersive X-ray analysis (EDAX) and time-of-flight secondary ion mass spectrometer (ToF-SIMS) measurements were performed to investigate the bulk composition. X-ray diffraction (XRD) was used to evaluate the phase and crystallinity of the deposited TDML films. Residual stress in these films was found to be significantly low. These TDML films were found to have excellent nanomechanical properties with maximum hardness of 41.2 GPa. In addition, various nanomechanical parameters were calculated and correlated with each other. Owing to metallic interfacial layer of Ti in multilayer films, the optical properties, electrical properties, and photoluminescence were improved significantly. Due to versatile nanomechanical properties and biocompatibility of DLC and DLC based films, these TDML films may also find applications in biomedical science.

**KEYWORDS:** thin films, nanomechanical properties, optical properties, electrical properties, biomedical applications, SEM, SIMS



## 1. INTRODUCTION

Now a days, cobalt–chromium (Co–Cr) alloys and titanium (Ti) based coatings are among the widely used materials for bioimplants (such as orthopedic implants), whereas nickel–titanium (Ni–Ti) alloys are considered as an excellent material for the development of a biomicroelectromechanical system (B-MEMS) due to their better mechanical and wear properties as well as shape memory effect in Ni–Ti alloys.<sup>1–3</sup> In spite of being efficient materials, most of them have certain drawbacks such as release of metal ions with time, toxicity,<sup>4,5</sup> corrosion, etc. Nickel, a widely explored metal in the biomedical applications, is found to be a highly toxic metal and its inclusion in the human body may lead to dangerous diseases like tumors, asthma, and even cancer.<sup>6</sup> As far as orthopedic implant is concerned, besides biocompatibility, the biomedical material must have excellent mechanical and wear resistance properties as well as better stiffness. Hydrogenated amorphous carbon (a-C:H) or diamond-like carbon (DLC) thin films have attracted considerable scientific and industrial attention of researchers due to their excellent mechanical and tribological properties.<sup>7,8</sup> The DLC has already been considered as an excellent biocompatible material, and its biocompatible properties have been studied extensively.<sup>1–3,6</sup> Thus, DLC can be an ideal candidate for biomedical applications. DLC films can be used in various ways to reform the drawbacks of existing biomedical material. For example, DLC coating can be used as hard and protective coating on NiTi B-MEMS, which

may further restrict the release of toxic Ni ions during uses of such machines in the human body. Similarly, it can also be deposited on Co–Cr alloys to enhance the life of bioimplants. DLC coatings also restrict the growth of bacteria; thus, it can enhance the life of medicine kept in the poly ethylene terephthalate (PET) and glass bottles.<sup>9</sup> It is to be noted that the hardness ( $H_N$ ) of DLC coatings varies in a range of 20–30 GPa that is comparable to Ti based coatings and is significantly higher than other biomedical materials. However, further improvement in hardness and wear resistance properties of DLC coating can enhance the life of bioimplants, especially orthopedic implants significantly. Since Ti and DLC both are very hard materials and have good biocompatibility, the use of these two materials in one structure can be very beneficial for biomedical applications.

In another aspect, versatile electronic structure and higher transmission of DLC made it also a smart material for electronic and optical applications.<sup>10–12</sup> However, DLC film exhibits high resistivity and low carrier mobility, which restrict its uses for optoelectronic applications such as solar cells. Actually, photo-generated charge carriers in DLC film recombine easily due to its high resistivity and low mobility; therefore, DLC films do not show photocurrent. In addition, DLC film shows high absorbance

**Received:** July 19, 2011

**Accepted:** September 26, 2011

**Published:** September 26, 2011

in deep ultraviolet (DUV) and UV regions but poor absorbance in the visible region. However, as far as photovoltaic application is concerned, its absorbance must be enhanced in the visible region. Besides this, DLC films have a major drawback of high residual stresses (RS), which restricts the growth of thicker DLC films and prohibits its industrial applications. Kumar et al.<sup>13</sup> have proposed the solutions to high RS. Nitrogen incorporation in DLC reduces the high level of RS at the significant expense of  $H_N$ . For avoiding such a problem, novel metal/DLC bilayer and multilayer were found to be an appropriate approach. Recently, we<sup>14</sup> have proposed Cu/DLC bilayer structures to minimize a high level of RS. These metal/DLC multilayer structures can not only minimize RS but also improve the nanomechanical, transport, and optical properties of the structure. Moreover, such a multilayer structure may provide unique microstructure (pure DLC films generally showed amorphous morphology). However, while preparing the metal/DLC multilayer structure, one has to be very careful about selecting an appropriate metallic layer. For example, in the case of Al/DLC multilayer structure, Al is a softer material and it has very high diffusivity into Si. Thus, this is not a desired metal/DLC multilayer structure because it may have very low  $H_N$  due to the soft nature of the material and very high RS due to high diffusivity into Si. Thus, there is a great interest to optimize the metallic layer to obtain desired properties from the metal/DLC multilayer structure. Recently, we<sup>15</sup> have also minimized RS and improved the electronic properties by employing Cu/a-C:H multilayer structure but at the expense of mechanical properties. Since Ti is a very hard metal and has a high barrier against diffusivity, the Ti/DLC multilayer structure can be better to obtain improved properties. Therefore, in the present study, we have grown different Ti/DLC multilayer (TDML) films and explored their possible multiple applications. For this, we used several characterizations.

## 2. MATERIALS AND METHODS

### 2.1. Materials and Ti/DLC Multilayer Sample Preparation.

TDML films were deposited using a hybrid system combining radio frequency (RF)-sputtering and RF-plasma enhanced chemical vapor deposition (PECVD) techniques, in the sequence of alternate layers of Ti and DLC, on well-cleaned Si wafers, corning 7059 glasses and stainless steel substrates. The schematic representation and description of a hybrid system used for the growth of TDML films can be found elsewhere.<sup>15</sup> These substrates were also cleaned in Ar plasma for 10 min prior to TDML films deposition. The base pressure for deposition of these multilayer films was kept at  $\sim 1 \times 10^{-3}$  Torr, which was achieved by a root-blower pump backed by rotary pump. Ti disk of 50 mm diameter was used as metal sputtering target, and the sputtering was performed on maintaining substrate to metal target distance at about 6 cm. The Ti layers in the multilayer films were deposited at constant negative self-bias and Ar gas pressure of 300 V and 70 mTorr, respectively, by the RF-sputtering process. On the other hand, DLC layers were deposited on successive Ti layers at constant negative self-bias and  $C_2H_2$  gas pressure of 100 V and 28 mTorr, respectively, by the RF-PECVD process. Only the number of Ti/DLC bilayers (combination of 1 Ti and 1 DLC layer makes 1 Ti/DLC bilayer) varied from 1 to 4. The samples TDML-1, TDML-2, TDML-3, and TDML-4 contain 1, 2, 3, and 4 bilayers, respectively.

### 2.2. Characterizations of Ti/DLC Multilayer Films.

The thickness of Ti/DLC multilayer films was evaluated by the Taylor-Hobson talystep instrument. The thicknesses of TDML-1, TDML-2, TDML-3, and TDML-4 were found to be  $\sim 227$ ,  $\sim 277$ ,  $\sim 312$ , and  $\sim 364$  nm, respectively. The thickness of the Ti layer was found to be  $\sim 20$  nm, whereas the growth rate for DLC layer deposition was found to

be  $\sim 44$  nm/min. X-ray photoelectron spectroscopy (XPS) analysis was carried out with Perkin-Elmer 1257 spectrometer having instrument resolution of 1 eV. Ti/DLC film was irradiated with X-ray of Al  $K\alpha$  1486.6 eV. Ti layer covered always under DLC layer; therefore, 5 min sputtering was also performed in order to visualize the underlying Ti layer. Energy dispersive X-ray analysis (EDAX) was used to examine the bulk composition such as Ti and C in the multilayer films. An X-ray diffraction study was performed using a Rigaku Miniflex diffractometer. The depth profile of TDML film with 4 bilayers was taken using a time-of-flight secondary ion mass spectrometer (ToF-SIMS) from ION-TOF GmbH, Germany. The secondary ions were generated because of bombarding pulsed primary ions from a 25 keV  $Bi^+$  liquid-metal ion gun (LMIG). Overall, the depth resolution was found to be better than 1 nm. A scanning electron microscope (SEM Leo Electron Microscope model 7060) was used to study the microstructure of multilayer films. The residual stress (RS) was measured using the 500TC temperature controlled film stress measurement system (M/s FSM Frontier Semiconductor, USA). The Stoney formula,<sup>11,12,14,15</sup> which is based on curvature method, was used to estimate RS. This is given by

$$RS = \frac{E_s d_s^2}{6(1 - \nu_s) d_f} \left[ \frac{1}{R_f} - \frac{1}{R_0} \right] \quad (1)$$

where  $E_s$ ,  $\nu_s$ ,  $d_s$ , and  $d_f$  are Young's modulus, Poisson ratio, thickness of the substrate, and thickness of the film, respectively, and  $R_0$  and  $R_f$  are the radii of substrate curvature before and after film deposition. Fully automatic software controlled IBIS nanoindentation (M/s Fisher-Cripps laboratories Pvt. Limited, Australia) having triangular pyramid diamond Berkovich indenter with normal angle of  $65.3^\circ$  between tip axis and the faces of triangular pyramid and curvature of  $150$ – $200$  nm at tip was employed to measure the nanomechanical properties of TDML films. The maximum indentation load of 10 mN was applied in nano-indentation testing. Optical properties such as transmission and absorbance were measured using a Schimadzu UV-vis 1601 instrument. Photoluminescence (PL) of deposited multilayer film was recorded at room temperature by a Perkin-Elmer LS 55 spectrometer. Dark conductivity measurements as a function of temperature in the range of 293–501 K were performed using a Keithley 610C Solid State electrometer.

## 3. RESULTS AND DISCUSSION

### 3.1. XPS, EDAX, and X-ray Diffraction (XRD) Analyses.

XPS was used to investigate chemical composition and oxidation states of TDML film. XPS spectra for sample TDML-1 are shown in Figure 1a–d. The general scan (0–600 eV) as shown in Figure 1a reveals the presence of elements C, O, and Ti. From spectra, it is evident that the peaks of these elements were found at their usual positions, but the intensity of the Ti peak was found to be negligible in a general scan. Said et al.<sup>16</sup> have observed this type of discrepancy in Ti incorporated DLC film. Earlier, we have also observed negligible intensity of Cu in a general scan of XPS of a Cu/a-C:H multilayer structure.<sup>15</sup> Since XPS is a surface sensitive technique and Ti layer was always covered under DLC layer, no clear peak of Ti was obtained in a general scan. Hence, in order to visualize Ti in TDML film, 5 min sputtering was also performed and then a Ti 2P core level spectrum was recorded, which is shown in Figure 1c. Generally, pure Ti 2P<sub>3/2</sub> and 2P<sub>1/2</sub> peaks are observed at 453.8 and 459.95 eV, respectively. However, in the present case, these peaks are observed at 458.3 and 465.2 eV, respectively. Thus, the analysis of XPS result confirmed that these peaks also have a contribution of TiO<sub>2</sub> instead of pure Ti. In addition, the presence of TiC was also observed. The TiC layer may get formed at Ti/DLC interfaces. These results are in good agreement with the reported literature.<sup>17</sup> Further, from

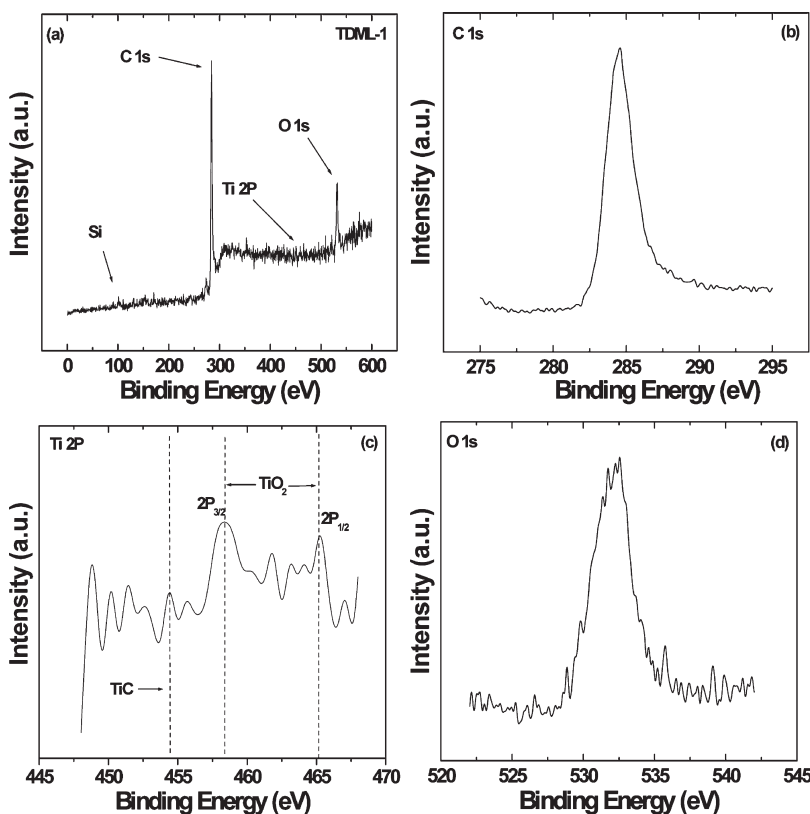


**Figure 1.** XPS spectrum of sample TDML-1 (a) general scan, (b) C 1s core level spectrum, (c) Ti 2P core level spectrum, and (d) O 1s core level spectrum.

core level spectra of O 1s, shown in Figure 1d, it was confirmed that these multilayer structures possess a significant amount of O. High base pressure growth condition was found to be a main cause for the presence of O in TDML film. Not only this but also some O may be attributed to the surface contamination during exposure of sample in air for loading it into the XPS chamber. Further, we have estimated the amount of oxygen by area of XPS peaks by considering the atomic sensitivity factors of different elements.<sup>18</sup> The amount of oxygen in this film (TDML-1) was found to be 9.1%. Nonetheless, such oxygen may help to improve the nanomechanical properties of Ti/DLC multilayer films due to the fact that oxygen plasma preferentially etches the soft graphite-like sp<sup>2</sup> clusters.<sup>19</sup>

Since XPS is a surface sensitive technique and, in a Ti/DLC multilayer structure, Ti layer always was covered under DLC layer, the EDAX and ToF-SIMS measurements were also performed in addition to XPS. EDAX uses high energy X-ray and provides information from the bulk of the structure. An EDAX spectrum of sample TDML-1 is shown in Figure 2a. The C and Ti were found to be two main elements in the deposited structure. Of course, the intensity of C was found to be greater than Ti. In addition to C and Ti, O and Si also appeared in the spectrum. The reason for the O peak has already been discussed in the XPS section. The high intensity Si peak confirms that high energy X-ray penetrated the film and reached the substrate.

XRD study was also performed to confirm the phase and crystallinity of the deposited film. Typical XRD spectrum of a TDML film with 1 bilayer (TDML-1) in the  $2\theta$  range of 10–60° is shown in Figure 2b. This spectrum reveals two main and sharp peaks at 33° and 42.4°, which correspond to Si  $\langle 200 \rangle$  and TiC  $\langle 200 \rangle$ ,

respectively. Si peak was due to substrate as the high energy X-ray penetrates the film, which was also confirmed by EDAX analysis. However, the TiC peak was due to the formation of the mixed TiC layer (TiC phase) at the Ti/DLC layer interface, which was also confirmed by XPS analysis. In addition, spectra show a broad hump corresponding to carbon in the range of 20–30°. On the other hand, three other peaks originating at 51.2, 54.6, and 56.3° are assigned to carbon, carbon  $\langle 004 \rangle$ , and TiO<sub>2</sub>, respectively. The results are in good agreement with the reported literature.<sup>20–22</sup>

**3.2. ToF-SIMS Analysis.** ToF-SIMS is a high resolution destructive technique and provides elemental information even from depth of the material. A typical ToF-SIMS depth profile of C, Ti, H, and Si from the sample TDML-4 is shown in Figure 3a. The structure of this sample TDML-4 consists of 4 Ti and 4 DLC layers alternatively. Depth profile gives clear elemental demarcation between C, Ti, and H. H diffuses deeper into the silicon than other constituents. This can be explained by ion implantation theory, according to which the heavier elements lose their energy near the surface and hence their diffusion takes place only near the surface. In contrast, lighter elements lose their energy deeper in the substrate and, therefore, diffuse in the bulk of material. This is why H was diffused deeper in Si than the other one. Further, 4 steps of Ti at different timings were also observed in its depth profiles. In order to visualize these steps more clearly, we have plotted the depth profile of Ti solely against time, which is shown in Figure 3b. The figure clearly shows 4 small peaks of Ti at certain intervals marked as numbers 1, 2, 3, and 4. It is to be noted that peak 1 has the highest intensity because the Ti layer corresponding to this peak was situated just above the substrate Si. However, intensity of Ti peak was reduced continuously from

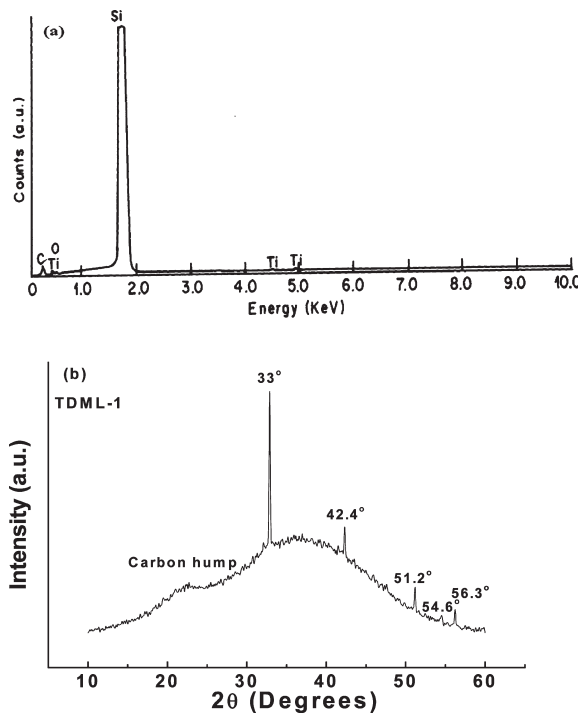


**Figure 2.** (a) Typical EDAX spectrum of TDML film having 1 bilayer (sample TDML-1), and (b) typical XRD spectrum of TDML film having 1 bilayer (sample TDML-1).

peaks 1 to 4, and peak 4 attains minimum intensity. Actually, before deposition of the first Ti layer (peak 1), no DLC layer was grown, and hence, no carbon gets deposited onto the target. In contrast, before deposition of second Ti layer (peak 2), one DLC layer was also deposited onto the substrate containing one Ti layer above its surface. Since during the first DLC layer deposition, some carbon also gets deposited onto the target Ti, during sputtering of the second Ti layer a comparatively thinner Ti layer may be deposited due to the fact that initially the carbon atoms get ejected from target and then Ti atoms. This is referred to as a target poison problem. Pauleau et al.<sup>23</sup> have explained this problem properly during investigation of Cu incorporated DLC films. Therefore, the intensity of peak 2 was found to be lower than intensity of peak 1. These processes continue with the further deposition of DLC and Ti layers and, hence, the intensity of Ti gets continuously reduced for peaks 3 and 4 also. Although Ti has a very high barrier against diffusion, a small fraction of Ti may also interdiffuse into Si. The interesting feature that is investigated by SIMS depth profile was the diffusion of C into Si. The depth profile of the pure DLC layer was also analyzed, which is shown in Figure 3c. A comparison of the depth profile of the DLC layer with the TDML-4 clearly infers that Ti layers in TDML reduce a significant amount of diffusion of C into Si. The restriction of diffusion of C into Si may reduce a high level of S and may improve various other properties such as electrical, optical, and nanomechanical properties of TDML films, which are discussed in the subsequent sections.

**3.3. SEM Analysis.** Surface morphology of TDML films with number of bilayers 1 and 4 is shown in Figure 4. SEM micrographs clearly reveal the nanostructured morphology in the TDML films. Since in all the TDML films the DLC layer was kept at the top and Ti layer was covered under this layer, the observed nanostructure was found to be a carbon nanostructure that was confirmed by EDAX analysis. Recently, we have observed generation of carbon

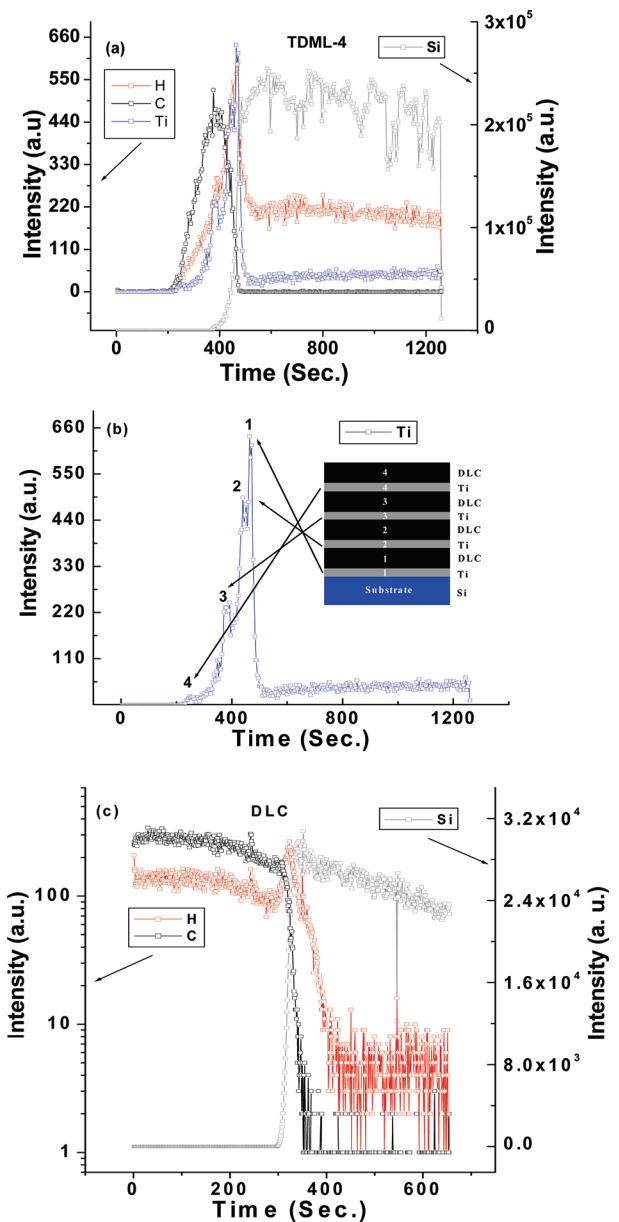


**Figure 3.** SIMS depth profile of (a) Ti, C, H, and Si from sample TDML-4, (b) only Ti from sample TDML-4, and (c) C, H, and Si from DLC film grown at 100 V.

nanostructures at the room temperature in Cu/a-C:H multilayer films.<sup>15</sup> Sample TDML-1 showed the room temperature growth of dense nanospheres, with diameter of 100–200 nm on the surface of the film. These nanospheres were so dense that besides isolated nanospheres they aggregated to form the clusters of spheres. These nanospheres were connected through the surfaces with other nanospheres. Recently, Du et al.<sup>24</sup> have observed the creation of such carbon nanospheres at high temperature ~500 °C. Further, increase in number of bilayers in TDML films led to drastic change in their surface morphology. TDML-4 film with 4 bilayers exhibited combined growth of the nanospheres and the rod-like carbon nanostructure on the surface of the film at room temperature. Actually, with increase in the number of bilayers, the thickness of TDML films also increased. Therefore, these nanospheres got aligned in such a way that they created a

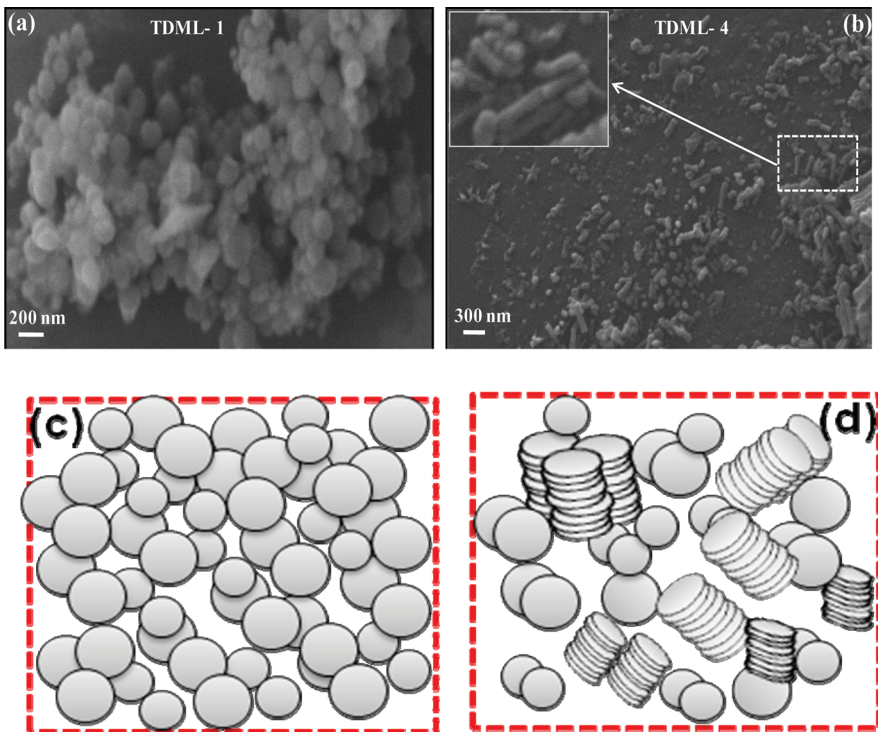


**Figure 4.** SEM micrographs of TDML films having number of bilayers (a) 1 and (b) 4. Schematic representation of growth mechanism of microstructure in samples (c) TDML1 and (d) TDML-4.

rod-like nanostructure. However, most of the nanospheres may not align properly, and hence, they were present as it is on the surface. This is the reason why TDML-4 film exhibited combined growth of nanospheres and nanorods. SEM micrograph of TDML-4 showed isolated as well as bundling of nanorods on the surface of film. SEM micrograph given in the inset of SEM micrograph of TDML-4 is the high resolution and high magnification picture from a specific location (as shown by rectangular box). These rods possessed 100–200 nm diameters, which is identical to the diameter of nanospheres. Thus, it is deduced that when a number of nanospheres are stacked on the top of one another precisely, then, they may give rise to the formation of high aspect ratio nanorods. We now discuss the transition of a nanosphere-like structure to a nanorod-like structure with the help of a hypothetical model for TDML-1 and TDML-4 samples, which are depicted in Figure 4c,d, respectively. Through this model, we propose a way for the creation of nanorods from nanospheres. It is well-known that a very thin layer of metal acts as a catalyst for growth of nanotubes and nanospheres.<sup>24–26</sup> Since TDML-1 contains 1 very thin interfacial layer of Ti, this interfacial layer may mold a successive DLC layer in such a way that a number of carbon nanospheres originates on various locations on the substrate. TDML-1 sample although revealed the formation of nanospheres which touch each other and showed an overlap, but due to only one DLC layer, these nanospheres did not get aligned in such a way to create uniform stacking. This results in generation of nanospheres only. On the other hand, if the number of metallic interfacial layers of Ti and successive DLC layers in TDML film increased (TDML-4), then all the interfacial Ti layers act as a catalyst for their successive DLC layers. Thus, each interfacial Ti layer helps to mold a successive DLC layer and generate nanospheres. When these nanospheres stacked precisely on one another, then they may give rise to the creation of nanorods, as

schematically presented in Figure 4d and confirmed by SEM micrograph (Figure 4b). It is not necessary that all the nanospheres stacked properly on one another in a multilayer structure with more bilayers. This is the reason why besides nanorods TDML-4 exhibited the generation of isolated nanospheres, which was observed by a SEM micrograph and presented schematically in Figure 4b,d, respectively. In addition, SEM micrograph (Figure 4b) also reveals the bundling of these nanorods. The most interesting fact regarding the creation of nanospheres and nanorods in the present study was that these nanostructures are formed at room temperature and Ti layer was employed as a catalyst to obtain such nanostructured morphology.

**3.4. Nanomechanical Properties.** The high resolution nanoindentation was used to measure the nanomechanical properties of TDML films. Besides TDML films, the mechanical properties of substrate silicon and reference sample fused silica were also investigated. Load versus displacement curves of TDML films grown under a varied number of bilayers from 1 to 4, fused silica and silicon substrate at indentation load of 10 mN are shown in Figure 5. It is clear that an increase in the number of bilayers from 1 to 4 increases the penetration depth continuously but TDML-3 and TDML-4 films show excellent recovery. Among various TDML films, the maximum plastic deformation was observed in TDML-2. However, fused silica exhibited maximum penetration depth. The penetration depth in all the TDML films was found to be lower than silicon and fused silica. Load versus displacement curves were employed to estimate hardness ( $H_N$ ), elastic modulus ( $E$ ), and various other nanomechanical parameters. The variation of  $H_N$  and  $E$  with the number of bilayers is depicted in Figure 6a,b, respectively.  $H_N$  in TDML films was estimated by composite hardness model.<sup>27</sup> The values of  $H_N$  for TDML films having number of bilayers as 1, 2, 3, and 4 were found to be 41.2, 28, 21.7, and 16 GPa, respectively. The  $H_N$  was

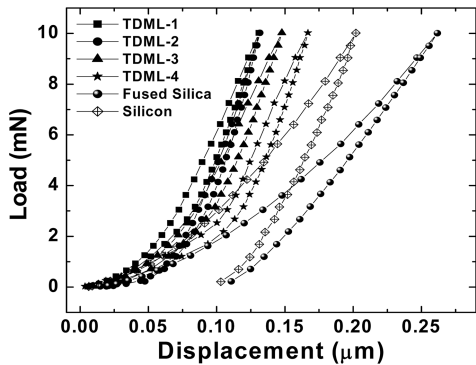


**Figure 5.** Load versus displacement curves of TDML films having number of bilayers 1, 2, 3, and 4, fused silica, and silicon.

found to continuously decrease with the increasing number of bilayers from 1 to 4. Thus, TDML-1 film with  $H_N$  41.2 GPa showed superhardness behavior. In contrast, recently, we<sup>12</sup> have observed maximum  $H_N$  only as 17.57 GPa in DLC film grown at 100 V. It is to be noted that, in the depositions of DLC films by RF-PECVD process, the substrates are generally kept at cathode, and C<sup>+</sup> and other hydrocarbon positive ions present in hydrocarbon plasma strike the substrate with significant energy. This creates interdiffusion of carbon ions into the substrate, as confirmed by SIMS analysis. This interdiffusion may lead to interfacial mismatch and therefore degrades the nanomechanical properties of DLC films. On the other hand, introduction of interfacial layer of Ti between Si and DLC (TDML-1) enhances  $H_N$  of Ti/DLC film significantly (maximum  $H_N \sim 41.2$  GPa). Recently, Xu et al.<sup>28</sup> have improved the mechanical properties of carbon nitride coating by Ti doping. In addition, Chen et al.<sup>29</sup> enhanced the hardness of TiC/a-C nanocomposite up to 31 GPa by increasing the Ti content, whereas Zhang et al.<sup>30</sup> observed hardness close to 31 GPa-32 GPa in nc-TiC/a-C nanocomposite. In contrast, Ti/DLC multilayer exhibited hardness better than these nanocomposites and seemed to be a simpler approach for the preparation of hard and superhard coatings. Moreover, recently, Batory et al.<sup>31</sup> deposited Ti/a-C:H bilayer and found significant improvement in mechanical properties especially in adhesion due to the bilayer approach. It is also important to note that the selection of appropriate interfacial layer is quite essential because properties and the nature of interfacial layer influence the nanomechanical properties of DLC films significantly. Recently, we<sup>15</sup> have also observed poor nanomechanical properties such as  $H_N$  in Cu/a-C:H multilayer films having bilayers from 1 to 4 because Cu is softer material and has good diffusivity in Si. Thus, not only were Cu/a-C:H multilayer films found to be softer but also they had sufficient interdiffusion of C into Si. On the other hand, the reason for higher  $H_N$  in TDML films (such as TDML-1) was that the interfacial layer of Ti is very hard and it may also form hard TiC bonding at the interface of Ti and DLC layers. In addition, Ti is also an excellent barrier to diffusion and, due to this characteristic, it is widely used in very large scale integrated (VLSI) circuit technology. Thus, Ti interfacial layer restricts the interdiffusion of C into Si and avoids the mismatch at the interface of Si and DLC. From SIMS analysis, it was clearly confirmed that TDML film has negligible interdiffusion of C than DLC film. Further, increase in stacking of two and three bilayers (TDML-2 and TDML-3) on Si made the structure unstable due to introduction of several interfaces into the film. These interfaces led to high plastic deformation that resulted into

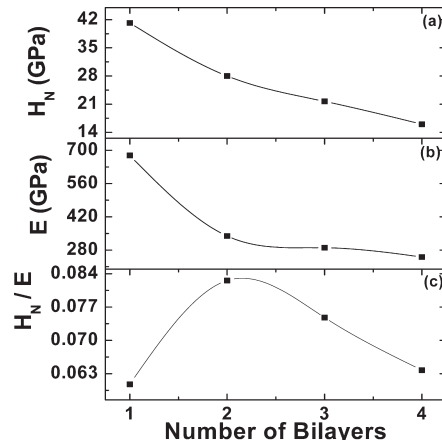


**Figure 6.** Variations of (a)  $H_N$ , (b)  $E$ , and (c)  $H_N/E$  with the number of bilayers of TDML films.

considerable reduction in  $H_N$  values. It is worth noting that up to a three bilayer structure (from TDML-1 to TDML-3), the  $H$  of TDML films was still higher than DLC films.<sup>12</sup> However, TDML film having 4 bilayers (TDML-4) exhibited a relatively lower  $H_N$  value, which was due to the further increase in interfaces into the film.  $H_N$  of all types of DLC films also strongly depends on ion energy. As ion energy varies linearly with self-bias, the self-bias controls  $H_N$  by controlling various bonding states in these films. Erdemir and Donnet<sup>8</sup> have classified the three energy levels to acquire the polymer-like, diamond-like, and graphite-like carbon films. They suggested the moderate ion energy for obtaining DLC coatings. The ranges of self-bias from 100 to 150 V have already been suggested by various authors to obtain DLC coatings. Moreover, we also observed diamond-like coating in the range between 100 and 125 V. This was the reason why growth of these multilayer films was performed at self-bias of 100 V. Further, observed  $E$  values followed the similar trend and were found to decrease continuously with the increase in number of bilayers from 1 to 4. The values of  $E$  in Ti/DLC multilayer films having bilayers 1, 2, 3, and 4 were found to be 677.8, 339, 290, and 251 GPa, respectively. Thus, TDML-1 film possessed not only maximum  $H_N$  but also maximum  $E$ . Besides TDML films,  $H_N$  and  $E$  values of silicon and fused silica were also evaluated. The values of  $H_N$  and  $E$  in silicon were found to be 10.4 and 130 GPa, respectively, whereas values of  $H_N$  and  $E$  in fused silica were found to be 9 and 78 GPa, respectively.

In order to elucidate elastic-plastic properties of TDML films further, the plastic resistance parameter ( $H_N/E$ ) was also discussed.<sup>7</sup> For high wear resistance coatings, the  $H_N/E$  ratio must be high. The limits of  $H_N/E$  for DLC based coatings varies in the range between 0 and 0.1, where the upper limit shows elastic behavior and high wear capability and the lower limit corresponds to the plastic behavior. The elastic-plastic combined behavior is encountered between 0 and 0.1. The variation of  $H_N/E$  against number of bilayers of TDML films is shown in Figure 6c. Initially on increasing number of bilayers from 1 to 2, the  $H_N/E$  ratio increases rapidly and attains a maximum value beyond which it gets continuously decreased for TDML films having 3 and 4 bilayers. The value of  $H_N/E$  was varied in the range of 0.061 to 0.082. Although TDML-2 film exhibited comparatively lower  $H_N$  than TDML-1 film, due to its observed maximum  $H_N/E$  value, this film may also have great application such as wear resistance coatings on magnetic storage media and

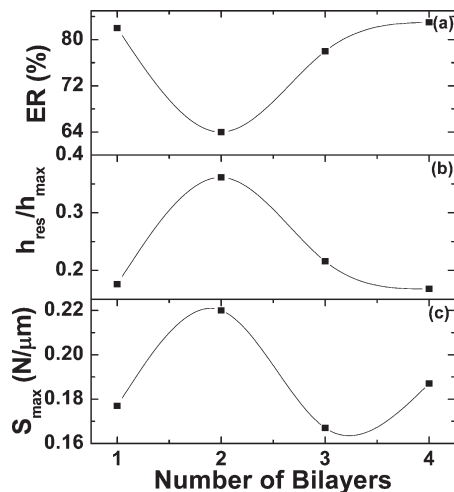


**Figure 7.** Variations of (a) ER, (b)  $h_{\text{res}}/h_{\text{max}}$ , and (c)  $S_{\text{max}}$  with the number of bilayers of TDML films.

biomedical implants. Further, elastic recovery (ER) in TDML films was estimated by employing the following relation<sup>7</sup>

$$\% \text{ER} = \frac{(h_{\text{max}} - h_{\text{res}})}{h_{\text{max}}} \times 100 \quad (2)$$

where  $h_{\text{max}}$  and  $h_{\text{res}}$  are the displacements at maximum load and residual displacement after load removal, respectively. Figure 7a shows the variation of ER with the number of bilayers of TDML films. Initially, ER was found to decrease with increasing number of bilayers from 1 to 2. However, further increase in number of bilayers led to significant enhancement in recovery, and TDML-4 film exhibited almost similar ER as observed in TDML-1. Actually, in 1 bilayer structure (TDML-1), the introduced interfacial layer of Ti prevents interdiffusion of C into Si and enhances ER. However, addition of one more bilayer (TDML-2) introduced some more interfaces, and indenter sees these interfaces during penetration. Thus, the plastic regimes develop at that point, which reduce the elastic deformation or ER. On the other hand, in the case of 3 and 4 bilayer structures, the observed increase in ER reveals the relaxation of bonding at interfaces. The ratio of residual displacement after load removal ( $h_{\text{res}}$ ) with displacement at maximum load ( $h_{\text{max}}$ ), i.e.,  $(h_{\text{res}}/h_{\text{max}})$ , provides information similar to that of ER with different domains of validity. Hence, this ratio was also calculated, and its variation with the number of bilayers is plotted in Figure 7b. The domain of validity of  $h_{\text{res}}/h_{\text{max}}$  varies between 0 and 1, where lower and upper limits correspond to elastic and plastic behaviors, respectively. The results of  $h_{\text{res}}/h_{\text{max}}$  were found to be in good agreement with ER results, and the film TDML-2 exhibited maximum plastic deformation. In addition, the unloading stiffness ( $S_{\text{max}}$ ) was also estimated for TDML films, and its variation with the number of bilayers is depicted in Figure 7c.  $S_{\text{max}}$  showed oscillating behavior in as grown TDML films. Initially, on increasing the number of bilayers from 1 to 2, the value of  $S_{\text{max}}$  goes up but it suddenly goes down for TDML film having 3 bilayers. However,  $S_{\text{max}}$  increases again for TDML film having 4 bilayers. The value of  $S_{\text{max}}$  was found to be in the range of  $0.167 \times 10^6$ – $0.22 \times 10^6 \text{ N}/\mu\text{m}$ .

The delamination of the film from the substrate due to high residual stress was found to be a major drawback of DLC films. In order to minimize such a high residual stress (RS), the TDML

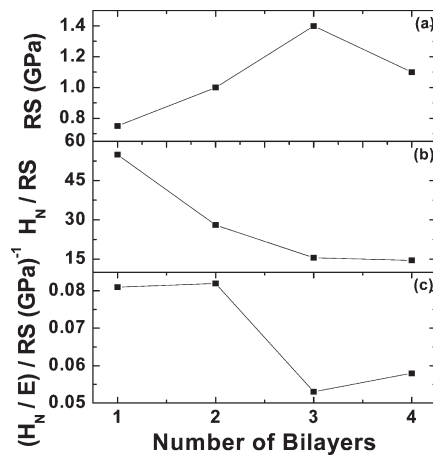


**Figure 8.** Variations of (a) RS, (b)  $H_N/\text{RS}$ , and (c)  $(H_N/E)/\text{RS}$  with the number of bilayers of TDML films.

films were grown in which number of Ti and DLC layers in alternative sequences were stacked on the top of one another. Several Ti layers present in TDML films acted as an adhesive layer for the successive hard DLC layer. Thus, one can obtain technologically challenged thick DLC films by employing TDML structure, because interfacial layers present in the multilayer structure reduce RS in the films as the Ti/DLC structure provides the needed relaxation in the overall structure. Figure 8a shows the variation of RS with the number of bilayers of TDML films. The value of RS in TDML films having a number of bilayers of 1, 2, 3, and 4 was found to be 0.75, 1.0, 1.4, and 1.1 GPa, respectively. Hence, it is seen that initially on increasing number of bilayers from 1 to 3 RS of the films was increased continuously but beyond 3 bilayer structure RS drops to a lower value. Previously, we have observed the similar trend of RS with a number of bilayers from 1 to 4 in Cu/a-C:H multilayer films.<sup>15</sup> However, the magnitude of RS in Cu/a-C:H multilayer was lower than TDML films. In fact, RS in Cu/a-C:H films was well below 1 GPa. Although RS in TDML films are comparatively higher than Cu/a-C:H multilayer films, it is considerably lower than pure DLC films because pure DLC films exhibit a very high RS of ~2 to 4 GPa and even more. Han et al.<sup>32</sup> have proposed that, in pure DLC or ta-C growth, the C ions strike the substrate and interdiffuse into Si. This leads to the formation of a SiC mixed layer at the interface, which results in interfacial mismatching and, hence, the interfacial stress. However, introduction of interfacial Ti layer prevents interdiffusion and avoids the formation of mixed SiC layer; this results in lower stress. On the other hand, observed comparatively higher RS in TDML films rather than Cu/a-C:H multilayer films<sup>15</sup> was due to the fact that Cu does not form carbide and, thus, avoids the formation of CuC types of any mixed layer at Cu and a-C:H layer interfaces. In contrast, Ti easily forms carbide and, hence, it may lead to the formation of mixed TiC layers at various Ti and DLC layer interfaces. Also, a Cu/a-C:H multilayer structure may possess more graphite-like  $\text{sp}^2$  bonding.

In DLC based thin films, generally high  $H_N$  is always accompanied by high RS; i.e., RS varies linearly with  $H_N$ . Thus, hardness per unit residual stress ( $H_N/\text{RS}$ ) was also evaluated to figure out the information about nanomechanical properties in depth due to a combined effect in TDML films. The higher the  $H_N/\text{RS}$  ratio (higher  $H_N$  and lower RS), the better is the quality of films.

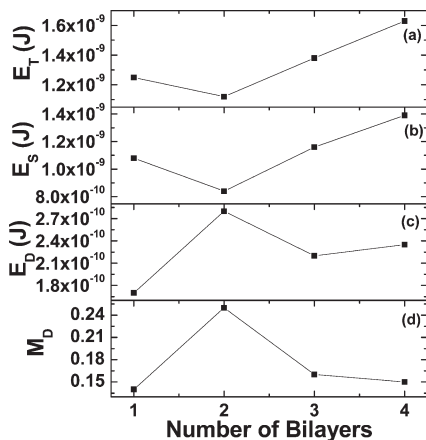


**Figure 9.** Variations of (a)  $E_T$ , (b)  $E_S$ , (c)  $E_D$ , and (d)  $M_D$  with the number of bilayers of TDML films.

Figure 8b shows the variation of  $H_N/RS$  ratio with the number of bilayers of TDML films. It is seen that initially  $H_N/RS$  decreased sharply with increasing number of bilayers from 1 to 2. However, beyond a 2 bilayer structure, the saturation in the values of  $H_N/RS$  was observed. Thus, among various TDML films, TDML-1 film exhibited maximum  $H_N/RS$  ratio and, therefore, it can be treated as better quality hard film. In addition, the plastic resistance parameter per unit residual stress  $[(H_N/E)/RS]$  ratio was also estimated, and its variation with the number of bilayers of TDML films is depicted in Figure 8c. Here, it is worth noting that  $H_N/E$  ratio in TDML-1 was significantly lower than TDML-2 but due to considering stress factor with wear resistance the values of  $(H_N/E)/RS$  ratio in TDML-1 and TDML-2 were found to be almost identical. Thus, not only TDML-2 but also TDML-1 was found to be an excellent wear resistance coating. The values of  $(H_N/E)/RS$  ratio were sharply reduced in TDML-3, and then, this ratio slightly increases in TDML-4. This is attributed to the change in value of RS in samples TDML-3 and TDML-4.

The elastic and plastic properties of TDML films were also explored in term of energy. Load versus displacement curves were employed to estimate the total deformation energy ( $E_T$ ), storage energy ( $E_S$ ), dissipation energy ( $E_D$ ), and modulus of dissipation ( $M_D$ ).  $E_T$  and  $E_S$  were calculated by integrating the loading and unloading curves, respectively, whereas  $E_D$  was estimated by taking the difference between  $E_T$  and  $E_S$ . The  $M_D$  was evaluated by taking the ratio of  $E_D$  and  $E_T$ . The variations of  $E_T$  and  $E_S$  with the number of bilayers of TDML films are depicted in Figures 9a,b, respectively. It is evident from Figure 9a that, initially on increasing the number of bilayers from 1 to 2, a slight reduction in the value of  $E_T$  is noticed but further increase in the number of bilayers to 3 and 4 leads to an enhancement in its value. The values of  $E_T$  were found in the range of  $1.12 \times 10^{-9}$ – $1.63 \times 10^{-9}$  J. Observed  $E_S$  values also followed the similar trend with the increasing number of bilayers (Figure 9b). The parameter  $E_D$  is very important while explaining the nano-mechanical properties of TDML films.  $E_D$  is basically a measure of plastic deformation during the loading–unloading profile. The variation of  $E_D$  with the number of bilayers of TDML films is shown in Figure 9c. The values of  $E_D$  in all TDML films were found to be lower and of the order of  $\sim 10^{-10}$  J. However, among the experimental four TDML films, TDML-2 exhibited a maximum value of  $E_D$ . This was in good agreement with the ER results because ER and  $E_D$  vary inversely with each other. In addition,

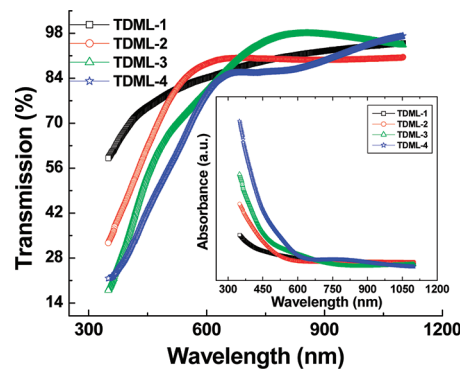


**Figure 10.** Transmission spectrum of TDML films having a number of bilayers from 1 to 4. The inset given shows the absorbance spectra of TDML films.

Figure 9d shows the variation of  $M_D$  with the number of bilayers of TDML films. Of course,  $M_D$  was found to be lower in these TDML films. Nonetheless, film TDML-2 exhibited a maximum value of  $M_D$ , which was found to be in good agreement with ER and  $E_D$  results.

**3.5. Optical Characterization of TDML Films.** Figure 10 shows the transmission spectrum of TDML films in the wavelength range of 350–1100 nm. The spectrum reveals the high optical transparency in visible and NIR regions which approaches above 90% despite the presence of very thin metallic Ti layer in the multilayer structure. Initially, on increasing the number of bilayers from 1 to 4, the overall transmission of TDML films goes down. However, it is not clear why the transmission of TDML-3 increases rapidly and attains the largest transmission beyond wavelength of  $\sim 660$  nm. The inset of Figure 10 is an optical absorbance spectrum of TDML films having a number of bilayers from 1 to 4. It is evident that the absorbance of these films was found to increase with increasing the stacking of number of bilayers. This is attributed to the enhanced thickness of the structure with the increase in number of bilayers. TDML film having 4 bilayers exhibited maximum absorbance. The most important issue with DLC and DLC based bilayer and multilayer structure is related to their usefulness to the photovoltaic applications. Generally, DLC films show maximum absorbance in DUV and UV ranges and very little in the visible range. Thus, in order to utilize it for photovoltaic application, the absorbance of DLC based structure must be enhanced in the visible region. It is very clear from the absorbance spectrum that, with the increase in number of bilayers of TDML films, not only the absorbance gets enhanced but also it is shifted toward the visible region. Thus, these TDML films may also be used in DLC based photovoltaic applications.

The variation of optical band gap ( $E_g$ ) with the number of bilayers of TDML films is depicted in Figure 11a. The values of  $E_g$  were estimated from Tauc plot  $(\alpha h\nu)^{1/2}$  versus  $\nu$  curve by taking the asymptotic/tangent of curve to the X axis. No significant variation in the values of  $E_g$  was observed, when the number of Ti/DLC bilayers was changed from 1 to 4. The value of  $E_g$  was varied in the range of 2.1–2.33 eV. Initially, on increasing the number of bilayers from 1 to 3, the value of  $E_g$  was increased from 2.1 to 2.33 eV, but beyond 3, the bilayer structure  $E_g$  was decreased and reached 2.2 eV for TDML film having 4 bilayers. The decrease in  $E_g$  beyond a multilayer having 3 bilayers might be due to an increase in  $sp^2$  bonding in carbon network because the

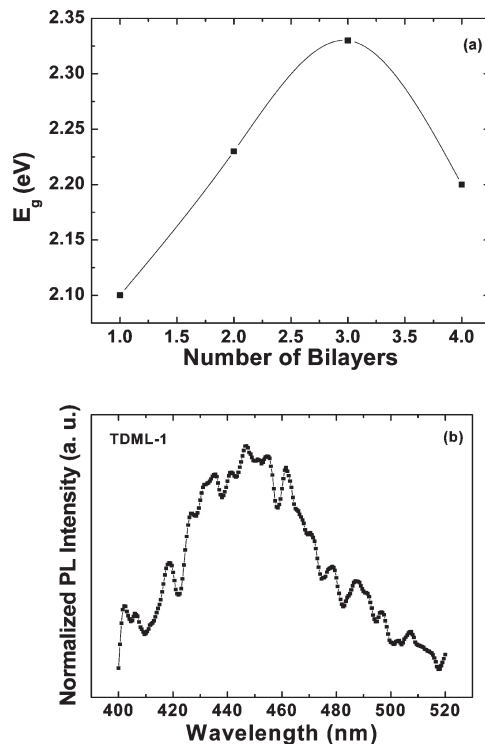


**Figure 11.** (a) Variation of  $E_g$  with the number of bilayers of TDML films and (b) typical PL spectrum of TDML film having 1 bilayer (TDML-1).

same trend was also observed in  $S$ , which also depends on  $sp^2$  bonding. Recently, we<sup>15</sup> have also observed the similar trend of  $E_g$  with the change in number of Cu/a-C:H bilayers from 1 to 4 in Cu/a-C:H multilayer films. It is also to be noted that  $E_g$  was found to be comparatively higher in TDML films than the Cu/DLC multilayer structure, which may be due to the fact that interfacial layers of Ti in TDML films helps to enhance more  $sp^3C$  bonding that broadens the  $E_g$ . Hardness results also support the said statement.

Due to low carrier mobility, the photoluminescence (PL) was found to be one of the versatile properties of DLC films.<sup>10</sup> The ability to tune PL emission over a wide range of wavelength may also lead to its diverse uses in the development of display devices. Theories regarding PL in DLC have already been proposed in the literature.<sup>33,34</sup> The PL property of DLC films strongly depends on  $\pi-\pi^*$  bonded  $sp^2$  clusters embedded in  $sp^3$  bonded matrix. Rusli et al.<sup>34</sup> have suggested that PL intensity in DLC films varies inversely with size of the  $sp^2$  clusters. Thus, larger cluster size shall lead to higher PL emission. Ti/DLC multilayer structure may be a novel approach to improve and tune its PL property. However, no explanation regarding PL in metal/DLC based multilayer structure was found in the literature. Typical PL spectrum of TDML film having 1 bilayer (TDML-1) in the range of 400–520 nm is shown in Figure 11b. From this figure, it is evident that a normalized PL spectrum shows a main broad peak in a visible range from ~410 to ~480 nm (indigo-blue edges), which comprises several small peaks. The main PL peak was centered at ~446.5 nm. This is to be noted that pure DLC film exhibits PL emission near 600 nm.<sup>33</sup> Thus, introduction of Ti interfacial layer shifts the PL emission toward a lower wavelength region (blue region). Interfacial Ti layer in Ti/DLC bilayer and multilayer structures may introduce

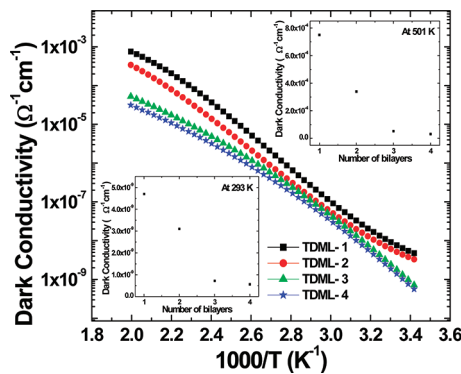


**Figure 12.** Variation of dark conductivity with the inverse of temperature for various TDML films. The figures given in the insets show the variation of dark conductivity at 293 and 501 K with the number of bilayers.

mid gap states, which therefore help to improve the PL property of these structures. In addition, the Ti/DLC multilayer structure involves a combination of metal and DLC layers alternatively. As the growth of the Ti layer was performed at a high base pressure condition, there may also be a possibility of formation of a  $TiO_2$  layer besides Ti. Thus, both DLC and metal layer may have different band gaps (probably, DLC will have a higher band gap than the oxidized metal layer). This difference in band gaps between these two layers may give rise to a well-like structure. Thus, photogenerated charge carriers may easily recombine in these wells rather than the normal DLC layer and may give rise to efficient PL emission. Observed shifting of PL peak from a higher wavelength region to a lower wavelength region may also be attributed to the creation of carbon nanostructures. We have also observed shifting of PL emission toward a lower wavelength region in case of Cu/a-C:H multilayer structure, where Cu/a-C:H multilayer films having 1 bilayer in its structure showed a main PL peak at ~447.5 nm.<sup>15</sup> In contrast, we observed shifting of PL emission toward a higher wavelength region for Si/DLC multilayer structure.<sup>35</sup> Thus, analysis of our PL results confirmed that additions of metal interfacial layers shift the PL emission of DLC toward a lower wavelength side.

**3.6. Electrical Property.** Temperature dependent conductivity of TDML films on coplanar structure was studied in the temperature range of 293–501 K, and its variation with the inverse of temperature is given in Figure 12. The TDML films followed a thermally activated process, which is given by  $\sigma = \sigma_0 \exp(-\Delta E_A/kT)$ , where  $\sigma$  is the dark conductivity and  $\sigma_0$  is the conductivity pre-exponential factors,  $\Delta E_A$  is the activation energy, and  $k$  and  $T$  are the Boltzmann constant and temperature, respectively. The conductivity of TDML films was found to continuously increase with the increasing temperature and showed semiconducting behavior. The conductivity of TDML-1 and TDML-2 films was varied in the range of  $\sim 10^{-9}$  and  $\sim 10^{-4} \Omega^{-1}cm^{-1}$ , whereas it was varied in the range of  $\sim 10^{-10}-10^{-5} \Omega^{-1}cm^{-1}$  for TDML-3 and TDML-4 films, with increasing temperature from 293 to 501 K. We have also observed high conductivity in n-type a-C:H/p-type crystalline Si diode.<sup>36</sup> In order to elucidate the role of the number of bilayers on conductivity of TDML films more clearly, the graphs of number of bilayers versus conductivity at 293 and 501 K were sketched and are shown in the insets of Figure 12. At 293 K, the conductivity was continuously decreased with the increasing number of bilayers

from 1 to 4. Conductivity at 501 K followed the similar trend and found to continuously decrease with the increasing number of bilayers. Of course an increase in bilayers increases the thickness as well as number of interfaces in the TDML films. Thus, a thermally generated charge carrier may get trapped in these interfaces and minimize the magnitude of conductivity. Also, with the increase in number of bilayers, the number of DLC and Ti layers in the TDML films is increased. As DLC layers have a lower mobility than Ti layers, this may give rise to lower conductivity in TDML films having more bilayers. Recently, we have observed higher conductivity in Cu/a-C:H multilayer films, but it also continuously decreased with increasing number of bilayers.<sup>10</sup>

It is worth noting that addition of interfacial Ti layers enhances the magnitude of conductivity in TDML films significantly. Recently, we have observed conductivity of  $\sim 7.6 \times 10^{-7} \Omega^{-1}\text{cm}^{-1}$  at 473 K in DLC films.<sup>12</sup> On the other hand, in TDML-1 film, where only Ti interfacial layer was added below DLC layer, the conductivity at 501 K was found to be  $7.5 \times 10^{-4} \Omega^{-1}\text{cm}^{-1}$ . Thus, the magnitude of conductivity in TDML films and Cu/a-C:H multilayer films was found to be more or less the same but significantly higher than the DLC films. Thus, metallic interfacial layers enhance the conductivity of DLC films. In addition, microstructures also play a vital role to influence the conductivity of TDML films. From SEM micrographs, it was clearly confirmed that the TDML-1 film showed generation of only nanospheres on the surface. In contrast, TDML-4 exhibited creation of both nanospheres and nanorods on the surface. Thus, in TDML-1 film, the thermally generated charge carriers see a uniform path to cover due to identical shaped structure (nanospheres) and they travel with identical velocity without any hindrance. This resulted in high conductivity in this film. On the other hand, in TDML-4 film, charge carriers see a nonuniform path due to existence of both nanospheres and nanorods, as they travel in both nanospheres and nanorods. Thus, due to the difference in structure, the charge carriers may not travel smoother than the previous structure and may result in comparatively lower conductivity in TDML-4 film.

#### 4. POSSIBLE APPLICATIONS OF TDML FILMS

Due to experimentally evaluated versatile nanomechanical, electrical, optical, and structural properties, TDML films may find wide applications.

**4.1. Biomedical Application.** TDML films exhibited super-hardness behavior having maximum hardness of 41.2 GPa and high wear resistance that is indirectly estimated by plastic resistance parameter. In addition, these films showed low stress and excellent stiffness. Due to these properties, TDML films can be widely used in biomedical applications. The most important biomedical application of TDML films may be in orthopedic implants. It is to be noted that when two closed surfaces (touching each other) start to move or rotate then low hard material gets scratched and damaged. Thus, the fraction of scratched material may mix into the human body and contaminate it. However, due to a very high hardness characteristic TDML films avoid such problems and are potential candidates for orthopedic implants such as knee, shoulder, and elbow joints. In addition, TDML films can be used as hard and protective coatings on NiTi based orthodontic archwires to protect the human body from release of toxic Ni ions. Furthermore, TDML films may also be employed as hard and protective coatings on heart valves due to their hard, wear resistance and biocompatible properties. Since DLC and

DLC based coatings have a gas barrier property and they also show very high transmission, medicines kept in PET and glass bottles may also get protected from bacteria and other contamination if one coats the DLC on the inner wall of these bottles. Due to DLC coatings, no oxygen will reach inside the bottles and, thus, any source for bacteria and other viruses to live inside the bottles is avoided. What is said for DLC coatings is also true for TDML films.

**4.2. Other Applications.** TDML films exhibited outstanding nanomechanical properties. Thus, these films can be used as hard and protective coatings on cutting tools, automobile parts, and wear resistance coatings on magnetic storage media. Due to semiconducting behavior with good conductivity, it can also be used in the semiconductor industry. Finally, due to excellent electrical, luminescence, and optical properties, these films have wide scope in the field of optoelectronic devices.

#### 5. CONCLUSIONS

We have used the hybrid system involving RF-sputtering and RF-PECVD techniques for the deposition of TDML films under a varied number of bilayers from 1 to 4. In these films, Ti interfacial layers acted as an adhesive layer and barrier to C diffusion into substrate. They also acted as a catalyst for the growth of nanospheres and nanorods, which were obtained at the room temperature conditions. These films showed comparatively lower S (which varied from 0.75 to 1.4 GPa), higher H (maximum 41.2 GPa), and improved optical and electrical properties. In conclusion, these TDML films may find their diverse applications such as hard, protective, and wear resistance coatings on the cutting tools, automobile parts, and magnetic storage media due to tremendous nanomechanical properties and solar cells due to better optoelectronic properties. These TDML films may also find their wider biomedical applications.

#### ■ AUTHOR INFORMATION

##### Corresponding Author

\*E-mail: skumar@nplindia.org. Phone: +91-11-45608650. Fax: +91-11-45609310.

#### ■ ACKNOWLEDGMENT

The authors are grateful to the Director, National Physical Laboratory, New Delhi (India) for his kind support. We gratefully acknowledge Dr. O. S. Panwar and Mr. C. M. S. Rauthan for their help. Authors wish to thank Dr. Govind, Dr. N. Karar, and Dr. K. N. Sood and Mr. Jai for providing XPS, SIMS, and SEM characterization facilities, respectively. N.D. acknowledges CSIR, Govt. of India for providing financial support through SRF fellowship. This research was sponsored by CSIR, Govt. of India, through the Network Project NWP-0027.

#### ■ REFERENCES

- (1) Catedege, S.-A.; Vaid, R.; Diggins, P., IV; Weimer, J.J.; Koopman, M.; Vohra, Y.-K. *J. Mater. Sci. Mater. Med.* **2011**, *22*, 307–316.
- (2) Roy, R.-K.; Ahmed, S.-F.; Yi, J.-W.; Moon, M.-W.; Lee, K.-R.; Jun, Y. *Vacuum* **2009**, *83*, 1179–1183.
- (3) Wang, J.; Jiang, N. *Diamond Relat. Mater.* **2009**, *18*, 1321–1325.
- (4) Savolainen, H. *Rev. Environ. Health* **1996**, *11*, 167–174.
- (5) Wataha, J. C.; O'Dell, N. L.; Singh, B. B.; Ghazi, M.; Whitford, G. M.; Lockwood, P. E. *J. Biomed. Mater. Res.* **2001**, *58*, 537–544.
- (6) Roy, R.-K.; Lee, K.-R. *J. Biomed. Mater. B* **2007**, *83B*, 72–84.

- (7) Erdemir, A.; Donnet, C. *J. Phys. D: Appl. Phys.* **2006**, *39*, 311–327.
- (8) Dwivedi, N.; Kumar, S.; Rauthan, C.-M.-S.; Panwar, O.-S. *Appl. Phys. A: Mater. Sci. Process.* **2011**, *102*, 225–230.
- (9) Katsikogianni, M.-G.; Syndrevelis, C.-S.; Amanatides, E.-K.; Matras, D.-S.; Missirlis, Y.-F. *Plasma Process. Polym.* **2007**, *4*, 1046–1051.
- (10) Robertson, J. *Semicond. Sci. Technol.* **2003**, *18*, 12–19.
- (11) Dwivedi, N.; Kumar, S.; Rauthan, C.-M.-S.; Panwar, O.-S. *Plasma Process. Polym.* **2011**, *8*, 100–107.
- (12) Dwivedi, N.; Kumar, S.; Malik, H.-K.; Govind, Rauthan, C.-M.-S.; Panwar, O.-S. *Appl. Surf. Sci.* **2011**, *257*, 6804–6810.
- (13) Kumar, S.; Dixit, P. N.; Sarangi, D.; Bhattacharyya, R. *J. Appl. Phys.* **1999**, *85*, 3866–3876.
- (14) Dwivedi, N.; Kumar, S. *Curr. Appl. Phys.* **2011**, DOI: 10.1016/j.cap.2011.06.013.
- (15) Dwivedi, N.; Kumar, S.; Ishpal; Dayal, S.; Govind; Rauthan, C.-M.-S.; Panwar, O. S. *J. Alloys Compd.* **2011**, *509*, 1285–1293.
- (16) Said, R.; Ali, N.; Ghumman, C.-A.-A.; Teodoro, O.-M.-N.-D.; Ahmed, W. *J. Nano Sci. Nano Technol.* **2008**, *8*, 1–7.
- (17) Meskinis, S.; Andrulevicius, M.; Tamulevicius, S.; Kopustinskas, V.; Slapikas, K.; Jankauskas, J.; Ciziute, B. *Vacuum* **2006**, *80*, 1007–1011.
- (18) Wagner, C. D.; Biggs, W. M.; Davis, L. E.; Moulder, J. F.; Muilenberg, G. E. *Handbook of X-ray photoelectron spectroscopy*; Perkin Elmer Corporation: Waltham, MA, **1979**.
- (19) Jiang, L.; Fitzgerald, A. G.; Rose, M. J.; Cheung, R.; Rong, B.; Drift, E. V. *Appl. Surf. Sci.* **2002**, *193*, 144.
- (20) Yang, H.-S.; Kwon, O.-H.; Lee, J.-D.; Kang, P.-H. *J. Ind. Eng. Chem.* **1996**, *2*, 106–115.
- (21) Iwashita, N.; Park, C. R.; Fujimoto, H.; Shiraishi, M.; Inagaki, M. *Carbon* **2004**, *42*, 701–714.
- (22) Kulish, M. R.; Struzhko, V. L.; Bryksa, V. P.; Murashko, A. V.; Il'in, V. G. *Semicond. Phys., Quantum Electron. Optoelectron.* **2011**, *14*, 21–30.
- (23) Pauleau, Y.; Theiry, F.; Barna, P. B.; Misjak, F.; Kovacs, A.; Dub, S. N.; Uglov, V. V.; Kuleshov, A. K. *Rev. Adv. Mater. Sci.* **2004**, *6*, 140–149.
- (24) Du, J.-M.; Kang, D.-J. *Mater. Res. Bull.* **2006**, *41*, 1785–1790.
- (25) Ikuno, T.; Yamamoto, T.; Kamizono, M.; Takahashi, S.; Furuta, H.; Honda, S.-I.; Ohkura, S.; Katayama, M.; Hirao, T.; Oura, K. *Phys. B* **2002**, *323*, 171–173.
- (26) Bonard, J.-M.; Croci, M.; Klinke, C.; Kurt, R.; Noury, O.; Weiss, N. *Carbon* **2002**, *40*, 1715–1728.
- (27) Johnson, B.; Hogmark, S. *Thin Solid Films* **1984**, *114*, 257–269.
- (28) Xu, P.; Li, J.-J.; Wang, Q.; Wang, Z.-L.; Gu, C.-Z.; Cui, Z. *J. Appl. Phys.* **2007**, *101* (014312), 1–4.
- (29) Chen, C. Q.; Pei, Y. T.; Shah, K. P.; Hosson, J. T. M. D. *J. Appl. Phys.* **2009**, *105*, 114314.
- (30) Zhang, S.; Bui, X. L.; Jiang, J.; Li, X. *Surf. Coat. Technol.* **2005**, *198*, 206–211.
- (31) Batory, D.; Stanishevsky, A.; Kaczorowski, W. *J. Acheiv. Mater. Manuf. Eng.* **2009**, *37/2*, 381–386.
- (32) Han, X.; Zhu, J.; Han, J.; Tan, M.; Gao, W. *Appl. Phys. A: Mater. Sci. Process.* **2008**, *91*, 529–533.
- (33) Pandey, M.; Patil, D.-S. *Diamond Relat. Mater.* **2007**, *16*, 1912–1917.
- (34) Rusli; Amaralunga, G.-A.-J.; Robertson, J. *Phys. Rev. B* **1996**, *53*, 16306–16309.
- (35) Dwivedi, N.; Kumar, S.; Rauthan, C.-M.-S.; Panwar, O.-S.; Siwach, P.-K. *J. Optoelectron. Adv. Mater.* **2009**, *11*, 1618–1626.
- (36) Kumar, S.; Dwivedi, N.; Rauthan, C.-M.-S.; Panwar, O. S. *Vacuum* **2010**, *84*, 882–889.